CFD Simulation of Reactive Flows: Catalytic Combustion in a Monolith

P. Canu and S. Vecchi
DIPIC, Università di Padova, 35131 Padova, Italy

Catalytic combustion in a structured catalyst was used to test advantages of computational fluid dynamics (CFD) codes with respect to simpler approaches to simulation of actual data and kinetic studies. Published experimental data on square channels and segmented monoliths were compared and used as a basis for parametric studies. The relevance of temperature-dependent transport properties was quantified. A comparison of 2-D approximations with a full 3-D model, which predicts a different ignition behavior, shows that the latter is needed to properly describe actual data. The segmentation of the monolith shows some influence on the overall combustion rate. The sensitivity analysis of the importance of chemical kinetics relative to mass transport suggests a need for a better description of surface mechanism, even if the simulated data are not uniquely under chemical control. A parameter-fitting procedure for kinetic studies based on the detailed 3-D, segmented CFD model was developed and successfully tested for modeling inhibition by water. Results show that more detailed surface and gas-phase reactions mechanisms must be included, but only after developing and validating a comparably detailed model of the momentum and heat transport in the actual geometry of the real process.

Introduction

Simultaneous modeling of reaction and flow is still a challenging problem for computational fluid dynamics (CFD) applications, where commercial codes lack quantitative predicting capabilities. Catalytic combustion in a structured catalyst is an interesting application where the advantages of CFD modeling can be evaluated, because it involves a fast reaction, that is very exothermic and is confined at the boundary of a flowing multicomponent mixture.

Catalyst-assisted combustion is recognized as a promising technology for cleaner heat and energy production. The catalyst allows the ignition of leaner fuel–air mixtures, resulting in a more stable combustion at lower temperatures, minimizing undesired reaction byproducts such as NO_x and CO. An effective way to arrange catalytic combustion is using a monolith reactor, also called "honeycomb reactor," where there are several small parallel channels, on the wall of which a layer of catalytic washcoat has been applied. The channels may have a variety of cross-sectional shapes, but the square one is the most common (Kolaczkowski, 1999). The substrate material is often either cordierite ($2MgO \cdot 2SiO_2 \cdot 5SiO_2$) or mullite ($3Al_2O_3 \cdot SiO_2$). Honeycomb reactors are extensively used in three-way automotive catalytic converters where the oxidation of carbon monoxide and unburnt hydrocarbons and the reduction of NO_x occur. For this purpose monolith reactors, with channels whose equivalent diameters are on the order of 1–2 mm, seem to be particularly appropriate. They have a fairly large surface area, and at the same time the pressure drop is limited (Geus and van Giezen, 1999). At present, the most promising application for catalytic combustion is the hybrid combustor to be used in natural-gas-fired turbines, where the formation of NO_x is a major concern (Forzatti and Groppi, 1999). Although commercialization is apparently at hand, there are still open issues concerning catalyst activity and durability under severe thermal-stress conditions. A proper design of the monolith requires that given temperature and conversion targets be reached at the reactor outlet. Besides the fundamental issue of a suitable catalyst identification and preparation, modeling can be extremely useful in sizing the reactor, understanding its behavior in operation, and predicting the effect of changing operating conditions. Temperature and fuel distribution in the channel are

Correspondence concerning this article should be addressed to P. Canu.

the basic information that determine the behavior of the whole monolith. Both variables are coupled since the combustion causes the temperature to rise, in turn increasing the combustion rate. The high temperature along the catalytic walls can deactivate and damage the catalyst. Knowledge about the temperature and fuel distribution may be acquired from experimental studies in a reactor operating at realistic conditions or from theoretical modeling studies in which the mass, heat, and momentum-conservation equations are solved using the proper reactor geometry. Experimental studies are expensive, particularly at the elevated pressure that is demanded by a gas turbine, while theoretical modeling studies need only a proper model formulation and adequate physicochemical data, where kinetics is the most uncertain information at the present.

There are several alternatives in modeling catalytic combustion systems (Pfefferle, 1995; Kolaczkowski, 1999). The simplest approach is a plug-flow reactor (PFR) model, where the surface reaction is applied to the whole section, even though it is surface-specific. Such a zero-radial-gradient model can be used only when the surface reaction controls the overall rate of the process ["micromixed" regime, according to Pfefferle (1995)]. Notwithstanding the approximation, the PFR model has been used to discuss a rather sophisticated surface-reaction mechanism. The rate of combustion at the surface increases quite easily to a level where the transfer of the reactants from the bulk to the surface cannot keep pace. At the same time, the heat released at the surface does not diffuse uniformly to the gas phase. In these conditions, the simplest model becomes a 1-D model that distinguishes surface and bulk averaged variables (Groppi et al., 1995). In this case, there is the additional uncertainty about the mass- and heat-transfer coefficients in the channel (Kolaczkowski, 1999) that depart from standard correlations in the literature because of entrance and surface reaction effects. Although dedicated correlations of transfer coefficients have been developed by comparison with more detailed models, utilization of the 1-D model is to be critically evaluated (Groppi et al., 1995). Detailed multidimensional models are required to correctly account for developing the spatial profiles of the variables. Beginning with the work of Young and Finlayson (1972), there have been a number of published 2-D models (Hayes et al., 1992; Markatou et al., 1993; Groppi et al., 1995) based on Navier–Stokes equations. Assumptions and solution methods differentiate the diverse approaches, while a limited verification against experimental data is common to them. The boundary-layer formulation is often used, that is, neglect of axial diffusion, to turn the differential equations in the simpler parabolic form, with great simplification in the solution methods. An interesting comparison has been attempted by Raja et al. (2000), including detailed surface chemistry. They concluded that boundary-layer and full Navier–Stokes 2-D models behave quite similarly, but the computation is much easier in the first case. It is surprising to observe the coupling of sophisticated chemistry models and the rather simplified description of the relevant features of the process, such as the catalyst temperature. In the calculation, a constant catalyst temperature is frequently assumed, which sounds like it contradicts the adiabaticity of the channel. The assumed wall temperature is quite common in the simulation, though (Pfefferle, 1995; Bond et al., 1996; Raja et al., 2000).

Among the many multidimensional formulations of the models, 3-D models are seldom used (Groppi et al., 1995; Jahn et al., 1997), even though some geometry, such as square and triangular channels, are intrinsically 3-D. Moreover, the combustion process behaves differently in these geometries, as shown later in this article. There is a common opinion that the equations for 3-D geometry become excessively tedious to solve. This is indeed the case if the complete numerical solution has to be developed for a specific geometry. In this work, we also try to demonstrate that actual monoliths, whatever the shape, can be easily modeled by means of commercial fluid-mechanics codes. The use of these design tools is rapidly expanding, and reactive flow problems constitute a challenging bench test. Moreover, computation obtained by means of widely accessible tools allows a simpler comparison of similar studies, on a reproducible basis. Several simplifying assumptions about the fluid mechanics and the boundary conditions can be dropped and advantage taken of robust and efficient numerical techniques, suitably developed for flow problems (Patankar, 1980). A complex model such as a 3-D, full Navier–Stokes formulation, can appear excessive in some limiting circumstances, where the chemical regime is approached. Nevertheless, one needs a complex model to prove that a simpler one can be used. To be properly used, CFD tools require some skill and understanding of the physical problem, but then allow to include almost any relevant physical and chemical process, thus, enabling the discussion of possible simplifications. Eventually, it is shown that CFD codes can be efficient enough to be used in kinetic studies, where several simulations need to be carried out in a sequence in order to identify the optimal kinetic parameters. It is also a good opportunity to validate the adequacy of the models by comparing them with actual experimental data.

Description of the Single-Channel Model

Monoliths are an array of regularly shaped channels. We address the most frequent case of the channel with a square section. Such a geometry inevitably requires three spatial coordinates to specify each point. Only a few advantages are brought by symmetry, since it is not axisymmetric. A proper simulation is, thus, 3-D, although results of 2-D representations are also discussed.

General assumptions made here for the model are:

- *Laminar flow.* The maximum value reached by *Re* in the simulation of experimental data (Bond et al., 1996) was less than 160.
- *Steady state.* All the experimental data used for comparison were taken after a steady regime was reached. In the experiments considered, no mention of multiple steady-states is made; in addition, distributed-parameter models do not predict multiple steady-state solutions if the contribution of the wall conductivity is not considered.
- *Only one channel needs to be simulated.* It is supposed that inlet conditions are the same for all channels, thanks to premixing, and that the catalytic activity of the applied washcoat is uniform.
- *Adiabatic channels.* If every channel behaves in essentially the same way, there is no heat exchange through the walls. Experimental measurements (Bond et al., 1996) con-

firm an adiabatic temperature following the conversion increase.

- *Nonconducting walls.* Thermal conductivity of walls is neglected. Particularly in the axial direction, this can be a seriously destabilizing process. The approximation is possible, since monoliths are made of low-conducting ceramic materials. The validity of the assumption is further discussed after the calculation results.
- *Neglect of heat flux by radiation.* This assumption is normally made in the literature (Groppi et al., 1995; Hayes and Kolaczkowski, 1999; Raja et al., 2000) on the basis of the high aspect ratio of the channels. We also make this assumption. Notwithstanding that, some contribution to heat the mixture can be expected, particularly in the warmer zones of the channel, where the temperature can easily go above 1,000 K.
- *Ideal gas.* The gas mixture is assumed ideal since pressure is usually low (less than 10 bars, frequently atmospheric), temperatures are elevated, and species are small, mostly nonpolar molecules. The maximum deviation is shown by steam at the inlet conditions considerated here: Z_{H_2O} (850 K, 1 bar) = 0.9994.
- *Negligible buoyancy.* Gravity is neglected because of the small vertical extent of the horizontal channels.
- *Neglect of homogeneous chemical reaction.* Since temperature is moderately high, gas-phase reactions do not occur in the first stage of the catalytic combustor.

The validity of some of the preceding hypotheses is discussed through simulations performed without applying them. Note that no assumption is made about velocity profiles, which are completely calculated by the model, including the developing-flow zone at the channel entrance and the subsequent modification caused by the heating of the surface. This is significant for proper mass-transfer modeling, particularly in the cases of segmented monoliths.

Conservation equations

According to the preceding assumptions, the basic conservation equations of the model are summarized below.

The continuity equation

$$\nabla\cdot(\rho\boldsymbol{U}) = 0 \tag{1}$$

The momentum conservation equation

$$\nabla\cdot(\rho\boldsymbol{U}\otimes\boldsymbol{U}) = \nabla\cdot\sigma \tag{2}$$

with the stress tensor

$$\sigma = -p\delta + \frac{2}{3}\mu\nabla\cdot\boldsymbol{U}\delta + \mu\left[\nabla\boldsymbol{U} + (\nabla\boldsymbol{U})^T\right] \tag{3}$$

The energy balance equation

$$\nabla\cdot(\rho\boldsymbol{U}H) - \nabla\cdot(\lambda\nabla T) = S_H \tag{4}$$

where

$$H = h_{\text{mix}}(T,p) + \frac{1}{2}U^2 \tag{5}$$

The species mass balance

$$\nabla\cdot(\rho\boldsymbol{U}Y_i) - \nabla\cdot(\rho D_{i,\text{mix}}\nabla Y_i) = S_i \quad i = 1, 2, \ldots, N_c \tag{6}$$

In addition, in order to complete the description, we need to know the ideal-gas equation of state

$$\rho = \frac{pW_{\text{mix}}}{RT} \tag{7}$$

and the thermodynamic enthalpy of the ideal-gas mixture

$$h_{\text{mix}}(T,Y) = \sum_i^{N_g} Y_i h_i(T) \tag{8}$$

with

$$h_i(T) = h_i(T_{\text{ref}}) + \int_{T_{\text{ref}}}^{T} C_{p,i}(T)\,dT \tag{9}$$

where $C_{p,i}(T)$, the specific heat of species i, is modeled as a polynomial function of temperature.

Note that the density is allowed to vary with temperature, pressure, and composition. Again, this is an extremely important effect to model, since extreme accelerations are caused by density variation with temperature.

Although the adoption of a single global reaction allows us to model a single component (typically the fuel), as is frequently done in the literature, we chose to solve all the species mass balances in order to correctly account for variations in the mixture properties (λ, μ, D, W, and h).

Boundary conditions

The calculations presented in the following include both parametric studies and a comparison with the experimental data of Bond et al. (1996), because of the detail provided there. We always used the same inlet and boundary conditions corresponding to a single set of experimental data obtained by Bond et al. (1996), and specifically the one in which conversion is significant ($\phi = 0.39$). In the experiments, natural gas is oxidized in a reactor formed by a commercial monolith (200 cells per square inch, square channels with 1.5×10^{-3}-m sides, and 3×10^{-4}-m wall thickness) with 2% of platinum in the washcoat. The monolith is segmented into four cylindrical wafers with a diameter of 0.05 m and a length of 0.02 m, leaving a 0.038-m empty space between for the measurements of intermediate temperature and conversion. Inlet conditions and measurements of conversion are summarized in Table 1.

For the solution of Eqs. 1–9, the uniform inlet velocity and composition were considered, with the values of Table 1, as was the uniform atmospheric pressure at the outlet. Walls are treated as adiabatic, not permeable, with no-slip on them, that is, the absence of any kind of flow (mass, heat, and momentum) at the walls.

Table 1. Inlet Conditions and Experimentally Measured Fuel Conversion at Different Axial Positions

	Inlet Conditions
Y_{CH_4}	0.0167
Y_{O_2}	0.171
Y_{H_2O}	0.0639
u [m/s]	7.3
z (m)	CH_4 Conversion (%)
0	0
0.02	10
0.04	40
0.06	55
0.08	63

Source: Bound et al. (1996).

Surface chemistry model

The heterogeneous reaction has been modeled as a single step: this approach allows the number of chemical-species mass-balance equations to be limited. However, single overall kinetics is an attempt to simplify the description of a complex phenomenon, but values of the kinetic parameters end up depending on operative conditions. A fundamental approach is the so-called microkinetic method described by Boudart and Djega-Mariadassou (1984) and applied by Dumesic et al. (1993) to several industrially relevant reactions. For the heterogeneous combustion of CH_4 on a platinum-based catalyst, the detailed mechanism suggested by Deutschmann et al. (1994) is often used in the literature. Many efforts have been made to develop detailed surface mechanisms for both palladium and platinum, but several aspects still remain unsolved: the estimate of kinetic parameters and the influence of a surface macrostructure are still rather uncertain. Verification of detailed surface mechanisms for combustion on supported catalysts against exp. data is quite scarce so far.

The global kinetic equation introduced in our model

$$R^S = A \cdot \exp\left(\frac{-E_a}{RT}\right) \cdot C_{CH_4} \cdot C_{O_2}^{0.5} \quad \left[\frac{kg_{CH_4}}{m^2 \cdot s}\right] \tag{10}$$

is the most frequently used equation (Markatou et al., 1993) for CH_4/air heterogeneous combustion on Pt. Besides parametric studies and fitting calculations, we always used $A = 273.85\ m^{5/2}/s \cdot kg^{1/2}$ and $E_a = 60.72$ kJ/mol, which derive from the best fit of the experimental data made by Canu (2001) with the same global kinetic equation and a 2-D model.

The commercial CFX code does not include surface reactions as a standard feature. The heterogeneous reaction taking place at the boundary of the domain is introduced through a source (or sink) term of material, S_i, and energy, S_H, at each boundary cell, especially referring to its outer surface (the catalyst wall). Accordingly, the ith species and the energy-balance equations are modified along the domain close to the wall. Source terms have the following expressions

$$S_i = \sum_{j=1}^{Nr} \nu_{ij} R_j^S \tag{11}$$

$$S_H = \sum_{j=1}^{Nr} (-\Delta H_j) R_j^S \tag{12}$$

and are added on the right side of Eq. 4 and Eq. 6, respectively. To improve the convergence of the numerical solution, source terms have been linerarized, according to the suggestions of Patankar (1980), with great advantage. Source terms are null everywhere away from the catalytic walls. An exception is the case of homogeneous reactions that would enter the conservation equations through source terms applied everywhere in the flow domain. In order to check the assumption of negligible gas-phase reactions, we made some calculations, including a simplified mechanism for homogeneous reactions. In particular, we added the following two-step mechanism

$$CH_4 + 3/2O_2 \rightarrow CO + 2H_2O$$

$$CO + 1/2O_2 \rightarrow CO_2$$

suggested by Dryer and Glassman (1972), with the kinetic equations and parameters obtained in the original work.

Geometry models

As already pointed out, the experiments of Bond et al. (1996) considered for comparison used a monolith with square channels. The same channel geometry is common to most commercial monoliths. Therefore, we developed a 3-D channel model, since a square section does not fit a 2-D axialsymmetric model. The geometry of the square channel remains tridimensional even if the computation domain is reduced by exploiting two symmetry planes, reducing the simulation to a quarter of the section, as shown in Figure 1. Three-dimensonal models are seldom found in the literature (Jahn et al., 1997), as they are deemed computationally expensive (Kolaczkowski, 1999). When a Navier–Stokes approach is used in the literature, the usual procedure is to reduce the problem to a 2-D description (Hayes and Kolaczkowski, 1994; Groppi et al., 1995; Bond et al., 1996; Raya et al., 2000). In those works, the square channel is modeled as a circular one to take advantage of axial symmetry, as shown in Figure 1. To reduce a square section to a circular one two equivalence criteria can be used, as depicted in Figure 2. Case A reflects the conservation of the total catalytic surface, which is probably the most relevant feature of the geometry, resulting in a circular section with a diameter larger than the side of the square. Case B keeps the same equivalent diameter, or the same cross-sectional area/wetted perimeter ratio, resulting in a diameter equal to the side of the square (circle inscribed in the square). Although Case A seems more physically grounded, Case B is the usual approach in hydraulics, and is frequently used in the literature (Groppi et al., 1995). Sometimes Case B is also justified by electron micrographs of a monolith section (Hayes and Kolaczkowski, 1994) that show a rounding off of the corners of the square section following the application of the washcoat. Nevertheless, the resulting geometry is not axisymmetric yet, calling again for a 3-D description. We carried out simulations with both 2-D models, in order to compare them with the 3-D model.

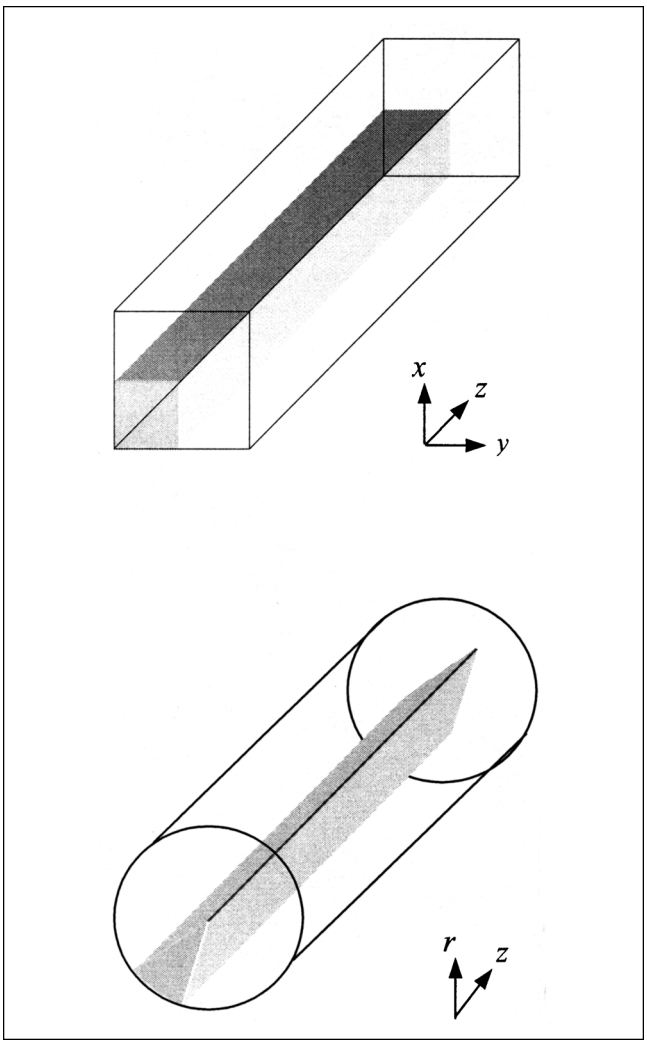

Figure 1. Computational domain (in gray) in both square and circular geometry and coordinates systems.

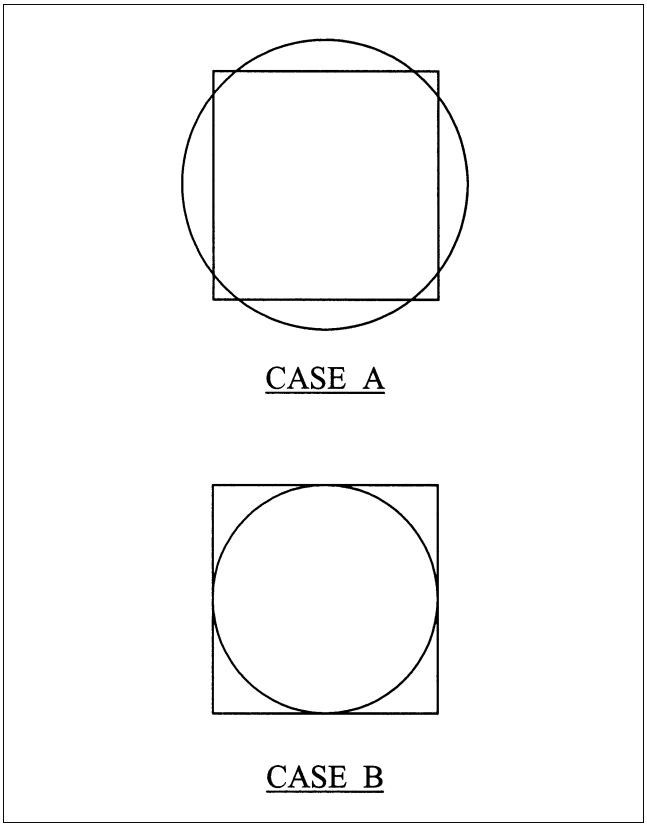

Figure 2. (Case A) 3-D vs. 2-D model with the same catalytic surface; (Case B) 3-D vs. 2-D with inscribed section.

Discretization of the domain

The computation domain highlighted in Figure 1 for both square and circular geometry is subdivided into finite volumes through a uniform mesh. We carried out simulations both with nonuniform meshes, which increased cell density in the regions expected to have the largest gradient (the catalytic surface and the inlet region), and with a larger number of cells. Results demonstrated that the algorithm implemented in CFX provides reproducible and reliable pointwise predictions of all the variables, with rather coarse and uniform grids also. The mesh refinement study has identified the best grid for 2-D models with 110×20 elements (0.727×0.0375 mm), and for the 3-D (square) model with $110 \times 20 \times 20$ elements ($0.727 \times 0.0375 \times 0.0375$ mm). With these grids, simulation of a typical experiment in the worst case of a 3-D model takes about 1 h on a Digital DS10 Server to converge from a generic initial guess at the solution. In the case where the results from a previous simulation on the same geometry are available, even if inlet conditions are different, the simulation can take a few minutes to converge, because the initial distribution of composition, temperature, and velocity in the channel is already shaped. Simulations were carried out using the commercial computational fluid dynamics (CFD) code CFX 4.4 of AEA Technology. The CFX software implements a finite-volume approach based on the work of Patankar (1980), with significant advancements. Results are available in the form of arrays of the local values for each unknown function (velocity components, pressure, temperature, density, each species' mass fraction, and transport properties, where variable) that can be easily visualized by means of intuitive colored maps, which are quite familiar to those using this kind of software. Since maps are mostly qualitative, we preferred to extract selected profiles of the solution functions, and frequently report results calculated from the CFD output, such as conversion, average values, or nonstandard profiles.

Transport Property Models

It is known that simulation results are quite sensitive to the evaluation of transport properties. Accordingly, constant properties provided by the CFD code have been replaced by detailed models for the calculation of transport properties. For this purpose we integrated the results from the Transport Library of Chemkin (Kee et al., 1994) in CFX, by means of polynomial interpolations.

Diffusion coefficients

Accuracy in modeling diffusion coefficients is crucial after the ignition of the surface reaction, since the combustion rate can then be larger than the reactant and product diffusion rates from bulk to surface and vice versa. We have tested three different diffusion-coefficient models of increasing complexity. We consider first the case of the binary diffusion coefficients of each component in nitrogen, because of the large amount of the latter. Coefficients were calculated according to the following equation (Hirschfelder et al., 1954)

$$D_{iN_2} = \frac{3}{16} \frac{\sqrt{2\pi k_B^3 T^3 / m_{iN_2}}}{p\pi\sigma_{iN_2}^2 \Omega(T)} \tag{13}$$

where temperature and pressure dependencies are accounted for, through such properties of the species as molar masses, m, collision integrals, Ω, and effective Lennard-Jones diameter for the collision, σ. Temperature dependency of each binary diffusion coefficient was calculated by means of Sandia's transport-properties prediction code of (Kee et al., 1994) and then interpolated through polynomials. Coefficients of the polynomials were then introduced in CFX by way of routines designed to allow the user to provide specific diffusion coefficients for each species. A more rigorous approach is the consideration of the full multicomponent approach to transport properties. Unfortunately, in this case, diffusion coefficients need a linear-system solution (Dixon-Lewis, 1968), the coefficients of which are temperature, pressure, and composition dependent. A workable solution is the mixture-average approximation. In this case, diffusion coefficients, $D_{i,\mathrm{mix}}$, still depend on the local composition, as well as to pressure and temperature, but the mixing rule is simpler

$$D_{i,\mathrm{mix}} = \frac{\sum_{k \neq i}^{N_c} y_k W_k}{W_{\mathrm{mix}} \sum_{k \neq i}^{N_c} y_k / D_{ik}} \tag{14}$$

We compared the effects of the two diffusion-coefficient models on the predictions of fuel conversion along the channel. Results are shown in Figure 3 for constant binary (in nitrogen) diffusion coefficients, evaluated at 1,000 K; temperature-varying binary diffusion coefficients; and mixture-average coefficients. The profiles obtained with mixture-average diffusion coefficients almost overlap the predictions of the temperature-dependent binary diffusion coefficients. Both differ quite significantly from the predictions with constant D_{i,N_2}. It can be concluded that the effect of the temperature on diffusion coefficients is much more important than the effect of composition, as modeled through the mixture-average approximation. The minor role of composition on the diffusion coefficients is reasonable under these circumstances, where we have lean combustion. On the other hand, the relatively small effect of switching from constant-diffusion coefficients to temperature-dependent ones (about 5% on the final conversion) is caused by the predominance of the chemistry on the transport processes with these conditions, mainly of the channel. A more detailed investigation on this point is reported in the following.

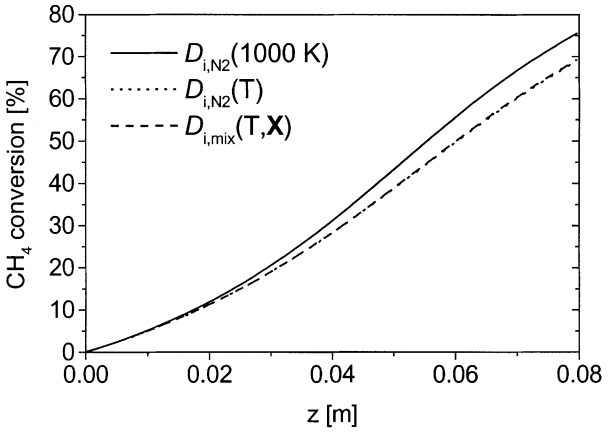

Figure 3. CH_4 conversion along the channel: comparison among different models of species diffusion coefficients.

Thermal conductivity

We initially conducted two tests with constant thermal conductivity, assuming the value of nitrogen for the whole mixture, evaluated at 850 and 1,500 K, respectively. We considered the wall temperature along the channel to compare the effect of different thermal conductivity models, since inaccuracies in heat-transport prediction in the gas phase close to the catalytic surface can seriously affect the wall temperature and then the rate of combustion. The individual species thermal conductivity is evaluated rigorously as a function of temperature by

$$\lambda_i = \frac{\mu_i}{W_i}\left(f_{\mathrm{trans}} C_{v,\mathrm{trans}} + f_{\mathrm{rot}} C_{v,\mathrm{rot}} + f_{\mathrm{vibr}} C_{v,\mathrm{vibr}}\right) \tag{15}$$

and it is composed of translational, rotational, and vibrational contributions, in turn, a function of μ_i, $C_{v,i}$, and the self-diffusion coefficient, D_{ii}, each one as a function of temperature (Kee et al., 1994).

Figure 4 shows that the value of thermal conductivity determines significant differences in wall temperature. Using the value of N_2 for the mixture thermal conductivity evaluated at 850 K results in catalyst temperatures that at some point can be more than 100 K higher than using λ_{N_2} (1,000 K). Note that λ_{N_2} (1,000 K) is only 15% higher than λ_{N_2} (850 K), but a low conductivity of the gas mixture does not allow the rapid removal of the heat of combustion from the catalytic surface.

Following these observations, we introduced a more complex model of mixture conductivity, as a function of temperature and composition, according to the mixture-average approximation (Kee et al., 1994)

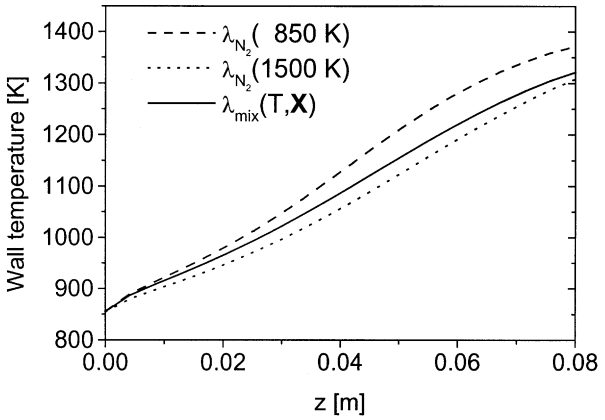

Figure 4. Temperature profiles of the catalytic surface: comparison among different models of mixture thermal conductivity.

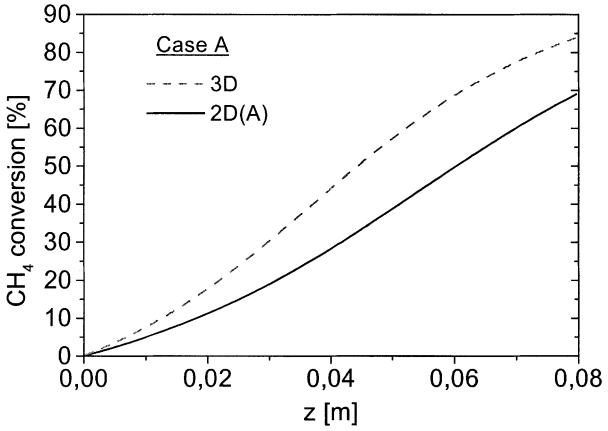

Figure 5. CH_4 conversion along the channel: 2-D vs. 3-D models; 2-D model with the same catalytic surface (Case A) of the 3-D model.

$$\lambda_{\text{mix}} = \frac{1}{2}\left(\sum_{k=1}^{n} Y_k \lambda_k + \frac{1}{\sum_{k=1}^{k} Y_k/\lambda_k}\right) \tag{16}$$

where each species thermal conductivity is evaluated as a function of temperature according to Eq. 15. The wall temperature profile obtained using Eq. 16 is also shown in Figure 4. As expected, the results are intermediate between the two preceding cases. Since these catalyst temperature differences can result in a final fuel conversion that can be up to 10% different, we performed all the simulations with the more detailed model provided by Eq. 16.

Viscosity

For completeness, the influence of viscosity on the model predictions was also verified. Two simulations were run in which the mixture viscosity was considered equal to that of nitrogen, evaluated to 850 K and 1,500 K, respectively. The viscosity of N_2 was evaluated through the standard kinetic theory expression (Hirshfelder et al., 1957)

$$\mu_i = \frac{5}{16}\frac{\sqrt{\pi k_B T m_i}}{\pi \sigma_i^2 \Omega(T)} \tag{17}$$

and varies between 3.73×10^{-5} and 5.4×10^{-5} Pa·s between 850 K and 1,500 K, leading to almost a 50% increase in the value. Notwithstanding that, the CH_4 conversion along the channel is so slightly influenced by molecular viscosity that profiles are almost indistinguishable. Accordingly we always used the value of nitrogen, at 1,000 K.

Results and Discussion

First we investigated the effect of the assumption about the geometry of the actual channel (2-D vs. 3-D models). The same kinetic parameters in Eq. 9 are used throughout all this analysis. It is clear from the superposition cross sections reported in Figure 2 that different results between the two alternative 2-D models described earlier (Cases A and B) should be expected, since radial diffusive paths can be quite different, as can be the flow structure. This is expected to affect both temperature and species distribution.

Comparison between 3-D and 2-D with the same catalytic surface (Case A)

In Figure 5, a comparison between 3-D and one 2-D (Case A) models is reported in terms of CH_4 conversion along the channel. It can be immediately noticed that this 2-D approximation significantly underestimates the fuel conversion throughout the whole channel, up to about 18% at the monolith exit. Also the local derivative of the conversion curves behaves differently, which is an indication of the local rate of fuel conversion. At first one could be led to explain the behavior of the 3-D model in terms of the diffusion limitations as the reaction gets faster, due to the longer paths between the axis and the corners. Sensitivity analysis, discussed later, proved that the physical processes in these conditions are not as relevant as one would expect. Before the disclosures of the sensitivity analysis, we explained the different conversion profiles by inspecting the temperature distribution in the channel. Figure 6 compares the surface temperature at the wall of the 2-D model along the channel with the same profiles at the surface of the square-channel model, at the nearer and farther lines from the axis. The surface in the 3-D model is noticeably hotter, especially in the corners. Apparently, there is a lack of convection in the corners to provide enough surface cooling. A stagnation zone forms at the corners, because axial velocity grows slowly along the diagonal of the square section. This is confirmed by Figure 7, where the axial velocity along the radial paths is reported for the two models. Both effects at the corners, a smaller axial velocity and a higher temperature, result in a longer residence time and a higher combustion rate, which leads to a higher fuel consumption per unit length. Interestingly, this also implies that the mass flowing close to the corners is smaller compared to

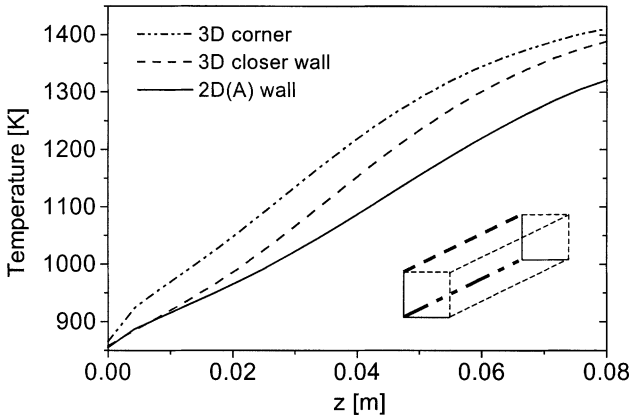

Figure 6. Surface-temperature profiles: 2-D vs. 3-D models.

2-D model with the same catalytic surface (Case A) as the 3-D model. 3-D profiles are reported for lines that are closer and farther from the axis, as indicated in the figure.

other zones of the square section. Accordingly, if the flow is radially segregated, one could expect that the overall fuel conversion is not affected by the higher activity at the corners because of a smaller flow rate in this area. Evidence to the contrary (Figure 5) implies that the exchange of mass in the radial direction is quiet efficient and that diffusion limitations are not an issue, as demonstrated in the following.

It can be concluded that circular and square geometry behave differently with respect to ignition, as already observed (Groppi et al., 1995; Wilson et al., 1992), and the role of corners in the square geometry is fundamental to promoting an earlier ignition of the mixture.

The resulting temperature profiles at the catalytic wall allow verification of the assumption of negligible axial conduction in the support. From Figure 6 an average axial temperature gradient of 7,500 K/m can be calculated. The thermal conductivity of the support is 1.4 W/K m (Boehman and Dibble, 2000), so that the total heat flux by conduction through the support is approximately 0.02 W, toward the channel inlet. The total convective heat flux carried by the gas in the flow direction varies along the channel, with an average value of 1.5 W, much higher than conduction in the solid phase, which can be neglected, as assumed in the beginning.

Comparison between 3-D and 2-D with inscribed section (Case B)

Modeling a square section through a totally inscribed circular one (Figure 2, Case B) can be justified by the actual structure of the washcoat, but in principle it cannot be compared with the original square geometry. We did it anyway because of the unexpected results discussed earlier. Note that the 2-D model results in a square section smaller than the 3-D model. Since the inlet boundary condition is given in terms of velocity, the two models are actually considering different flow rates. Seen in another way, the 2-D model reproduces only the inner part of the square channel, which in turn differs for the "extra" corners, as clear from Figure 2.

Results in terms of CH_4 conversion are shown in Figure 8. In this case, the 3-D model predicts a conversion increase slightly faster in the first part, but results get very close to those of the 2-D model toward the end of the channel. Allowing for an extra length beyond the actual dimension of the channel, the two models completely overlap. Such an unforeseen result deserves some further investigation. Figure 9 shows that the surface temperatures are almost the same, except in the corners of the 3-D model. Although a higher temperature in the corners was expected, the similarity of the temperature profiles at the same distance from the axis was not that obvious. Since the ratio between the perimeters (that are proportional to catalytic surface) is equal to $\pi/4$, just like the ratio between cross-sectional areas (proportional to inlet CH_4 flows), the only cause of the differences between the conversion profiles must be the "hot" corner zones. At the beginning, the corners anticipate the ignition, allowing the reacting mixture to remain there for a longer time because of a lower local gas velocity. This accelerates the combustion around the ignition region, as seen in Figure 8.

In the last part of the channel, according to the bending of the temperature profile shown in Figure 9, the combustion appears to be mass-transfer controlled at the corners. This is not consistent with a small effect of the geometry model, as shown in Figure 8, eventually indicating that the decrease in the combustion rate could not be caused by transport limitations. A conclusive argument on this issue will be given later in this work. A comparison between radial temperature profiles at different axial coordinates is shown in Figure 10. They confirm the preceding observations: in the first part of the channel the 3-D model predicts higher temperatures, because of the activity of the corners where the temperature is much higher. At the channel outlet, the temperature profiles overlap and the radial temperature gradient is smaller, once more contrasting with the hypothesis of transport limitations in this region.

Continuous vs. segmented monolith

Experimental investigations on catalytic combustion in monoliths frequently segment the monolith in order to obtain

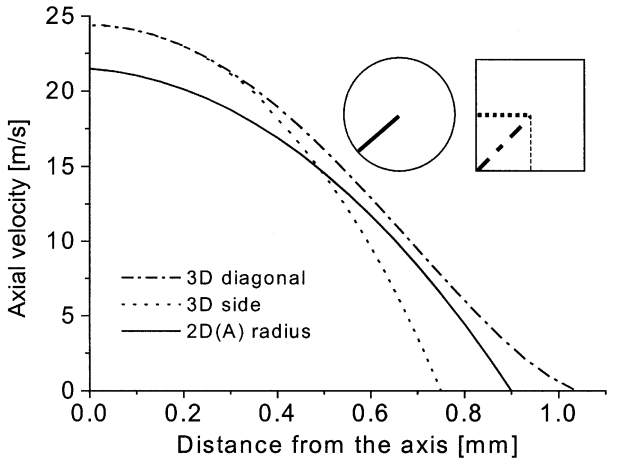

Figure 7. Axial velocity along radial paths: 2-D vs. 3-D models.

2-D model with the same catalytic surface (Case A) as the 3-D model. 3-D profiles are reported for the shorter and the longer (diagonal) paths, as indicated in the figure. $z = 0.08$ m.

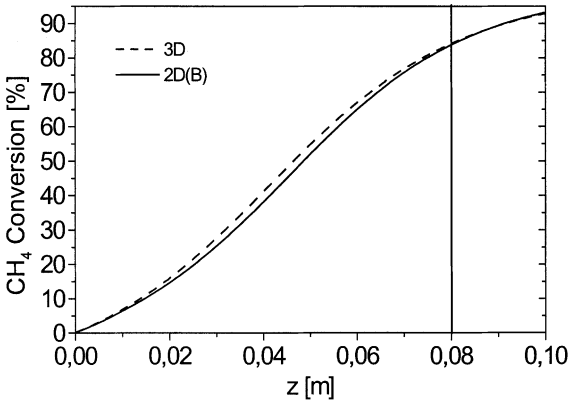

Figure 8. CH_4 conversion along the channel: 2-D vs. 3-D models.

2-D model with inscribed section (Case B). Profiles are extrapolated 0.02 m beyond the actual length of the channel, indicated by the vertical line.

intermediate measurements of temperature and composition. This is also true of the experimental data in the literature (Bond et al., 1996) on which we are basing our simulation. Segmentation is also a practical way of overcoming the vulnerability of ceramic monoliths to thermal shocks, since shorter pieces with lengths on the order of 0.02–0.03-m proved to be more resistant in industrial pilot applications (Ozawa et al., 1991; Furuya et al., 1987). On the other hand, simulation approaches tend to neglect this feature for simplicity, assuming a single continuous channel with a total length equal to that of the monolith. The results about the effect of geometry just shown were obtained using the continuous-channel approach. The purpose there was to compare the two geometries of the cross section. To compare those simulation results with the experimental data obtained in a segmented monolith, we must discuss the effect of the continuous-channel assumption. A sequence of interruptions of the channel is expected to destroy the structure of the flow

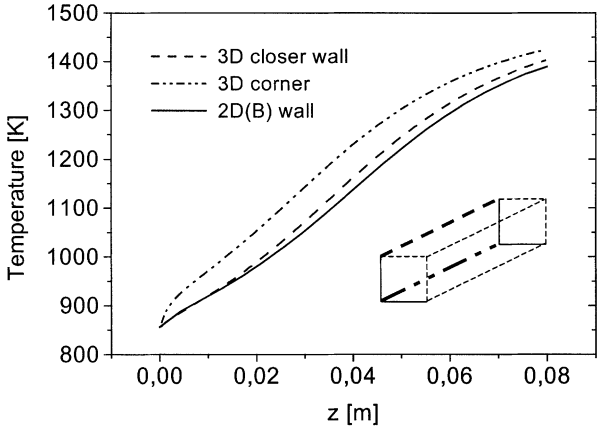

Figure 9. Surface temperature profiles: 2-D vs. 3-D models.

2-D model with inscribed section (Case B). 3-D profiles are reported for the lines closer and farther from the axis, as indicated in the figure.

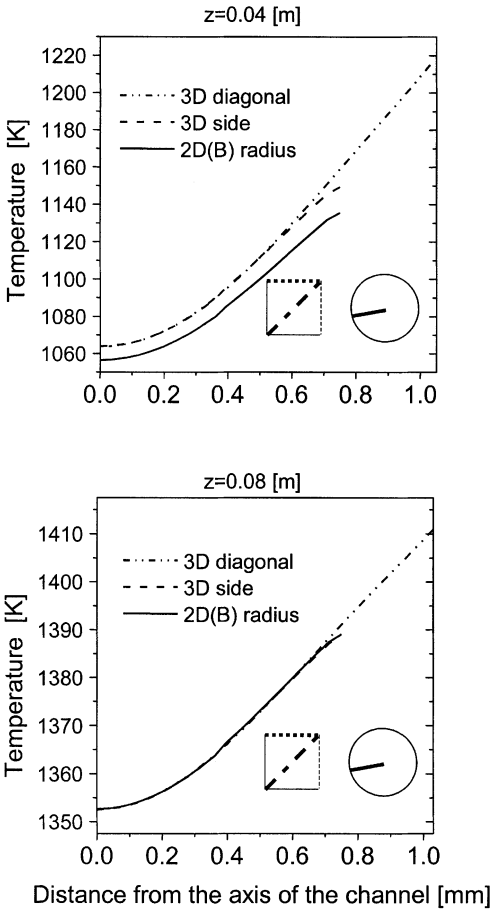

Figure 10. Temperature along radial paths: 2-D vs. 3-D models.

2-D model with inscribed section (Case B). 3-D profiles are reported for the shorter and the longer (diagonal) paths, as indicated in the sketch. Axial positions: half length ($z = 0.04$ m), top panel; channel outlet ($z = 0.08$ m), bottom panel.

and allow intensive mixing (Groppi et al., 1995). Since local values of temperature, composition, and velocity are so crucial, significant disturbances must affect the results.

To simulate the actual monolith (a sequence of four 0.02-m segments) inlet boundary conditions for all segments must be provided. In between two segments a perfect mixing has been assumed to take place. Resistance to the flow caused by the subsequent segment causes a flattening of the profiles of any variable in the transverse directions (x, y, or r, depending on the assumed geometry) on the whole monolith section. Accordingly, the average mass fractions of species i are given by

$$\overline{Y}_i = \frac{\int_A \rho u Y_i \, dA}{\int_A \rho u \, dA} = \frac{\int_A \rho u Y_i \, dA}{\dot{M}} \tag{18}$$

where transverse variations of axial velocity and density, in addition to those of Y_i, are properly accounted for. After mixing the temperature requires some assumptions about heat

transfer. It is reasonable to assume that mixing takes place adiabatically, that is

$$\dot{M}\overline{H}(\overline{T}) = \int_A \rho u H(T)\, dA \tag{19}$$

where a distinction between local, distributed variables (H, T), and the values after mixing ($\overline{H}$, $\overline{T}$) is made. Averaging the enthalpy is different than averaging the temperature because of the nonlinear dependence $H(T)$. Obtaining the average temperature from Eq. 19 requires solving the nonlinear equation. A simpler method to calculate the average temperature after adiabatic mixing makes use of the fuel conversion, ξ, and the rise in adiabatic temperature

$$\overline{T}(z) = T_{\text{in}} + \xi(z)\cdot(T_{\text{ad}} - T_{\text{in}}) \tag{20}$$

The resistances caused by the entrance in the following monolith segment flattens out the axial velocity profile, and the average value is given by

$$\overline{u} = \frac{\int_A u\, dA}{A} \tag{21}$$

The average values $\overline{Y}_i$, $\overline{T}$, and $\overline{u}$ calculated through Eqs. 18, 20 and 21 are then given as inlet boundary conditions to the next monolith segment.

A comparison between the conversion profiles predicted by the continuous and segmented channel models is shown in Figure 11. Small differences are observed with the catalyst and inlet conditions considered for these calculations, which are one set of the data of Bond et al. (1996). Conversion in a continuous channel is slightly higher, since the adiabatic mixing between segments decreases the heterogeneous reaction rate by cooling the gas that flows close to the surface. This can be clearly observed in Figure 12, where the temperature profiles at the surface are shown. Adiabatic mixing between segments levels the temperature over the whole section, causing quite a temperature drop on the catalytic surface for most of the subsequent segment. Such an effect is more sensible in the middle of the reactor (second and third segments) where the combustion rate increases faster (ignition zone). Here the temperature distribution is quite uneven, with the surface heating up while the bulk is much colder. Mixing in this case causes a sudden drop in temperature, which is particularly significant in the corners, the role of which is important in sustaining the ignition. At the same time, mixing equalizes this negative effect on the surface temperature by providing a means of increasing the fuel concentration at the surface soon after the entrance of each segment, in a region where the reaction is fast enough to begin starving the reactants. At higher conversion the decrease in the combustion rate reduces the differences between the continuous and segmented models. Now the temperature distribution is different, with the bulk temperature higher than before, so that mixing does not decrease the surface temperature so much. Also the corner zones, the role of which was found so important and whose temperature is particularly affected by mixing, are less disturbed by segmentation when the reaction has propagated enough. The transverse temperature distribution also affects the variation of D_{iN_2} that proved to be quite relevant for the combustion rate toward the last part of the channel, as is clear from Figure 3. It can be argued that the difference between the two models can be larger when the mass transfer is more a limitation factor.

Figure 13 shows the axial velocity profiles along the axis of the channel. It can be clearly seen that there is a developing

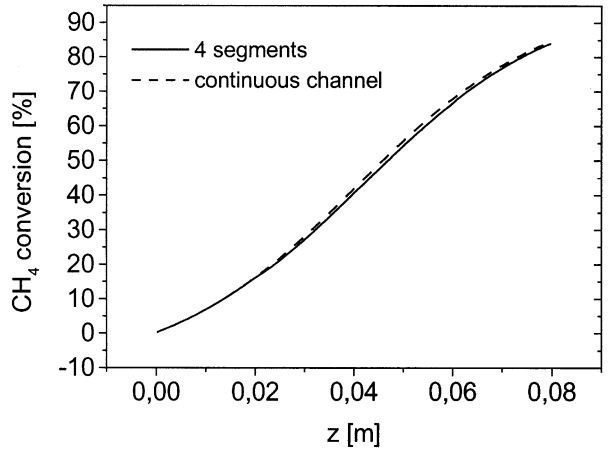

Figure 11. CH_4 conversion along the channel: continuous (dashed line) vs. segmented-channel models (solid line).

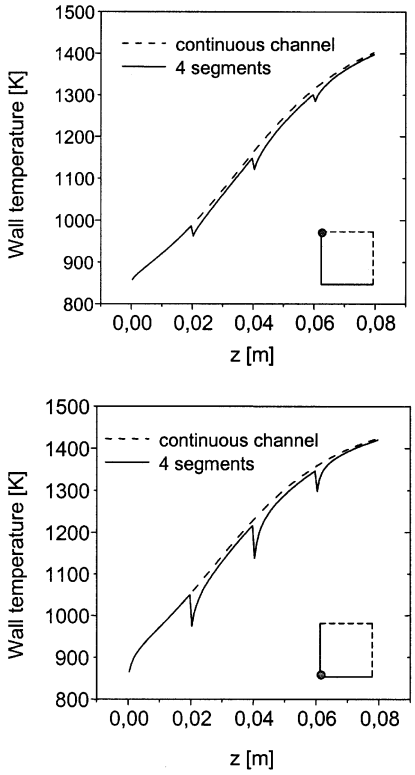

Figure 12. Surface temperature profiles: continuous vs. segmented-channel models.

Temperature at the surface closest to the axis, top panel, and at the corner, bottom panel.

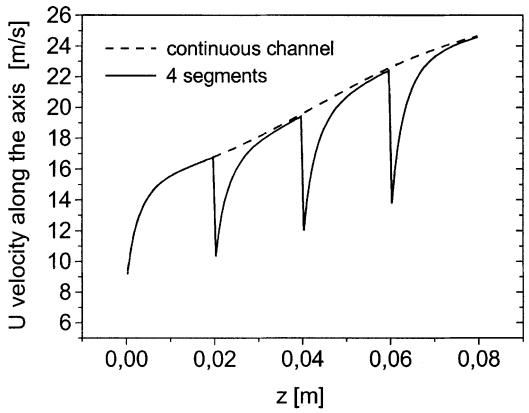

Figure 13. Axial velocity profiles along the axis of the channel: continuous- vs. segmented-channel models.

flow through a significant portion of each segment. This effect reduces the acceleration caused by the expansion due to heating the gas mixture, also observable in Figure 13 is the overall tendency of the velocity to increase along the channel. Although the value predicted by the continuous-channel model is eventually reached at the end of each segment, a lower axial velocity along the center line of the segmented monolith implies a higher value close to the catalytic surface, due to the developing boundary layer at each segment entrance, which evolves from a plug type of flow to a parabolic shape. This causes heat to be removed more efficiently from the catalytic surface, thus, keeping it colder and less reactive.

Gas-phase reactions

In order to assess the approximation introduced by the assumption of negligible gas-phase reactions, calculations have been carried out with the simplified mechanism,

$$CH_4 + 3/2\ O_2 \rightarrow CO + 2H_2O$$
$$CO + 1/2\ O_2 \rightarrow CO_2,$$

of Dryer and Glassman (1972). The reaction scheme just shown is quite a rough representation of the gas-phase chemistry, which is known to be much more complex, as reflected by the most recent version of GRI Mech (Frenklach et al., 1995). Nevertheless, we believe it can be a good starting point for getting an indication of the effect of the homogeneous reaction, without involving radical species in the model, while keeping the same degree of detail for both homogeneous and heterogeneous reactions. A comparative result is shown in Figure 14. As expected, the gas-phase reactions do not modify the result of the larger part of the transformation, and particularly when the temperature does not increase enough to trigger the homogeneous reaction. The precise onset of the gas-phase reaction could also be lower because of the heterogeneous activation of the active gas species. Radicals can be introduced in the homogeneous phase, thanks to the surface reactions. Such a coupling cannot be reproduced with the simple chemistry used here for both homogeneous and heterogeneous reactions. Again, the need for a more detailed accounting of both reactions emerges, provided the model for flow and heat transport is developed enough, as we did in this work.

Sensitivity Analysis

In the preceding sections, we frequently mentioned the effects that could be connected to the physical transport processes, in order to provide some explanation of the observed behavior. The onset of a transport-limited regime in catalytic combustion in structured catalysts is also frequently reported in the literature. Limitations due to transport processes can be expected, because the reaction takes place only at the boundary of the flow domain, and it is exothermic in a substantially adiabatic environment, which results in a temperature rise that exponentially accelerates the same reaction rate. Figure 15, where the axial profiles of CH_4 mass fraction at the corners and along the axis are reported, shows that large transverse gradients can be found in most of the reactor. Al-

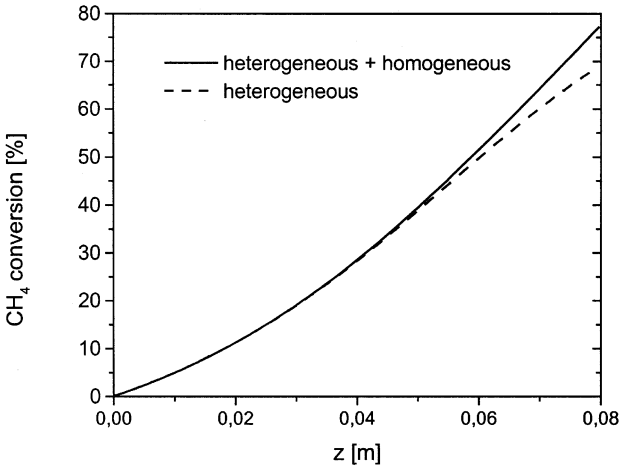

Figure 14. CH_4 conversion along the channel: effect of gas-phase reactions.

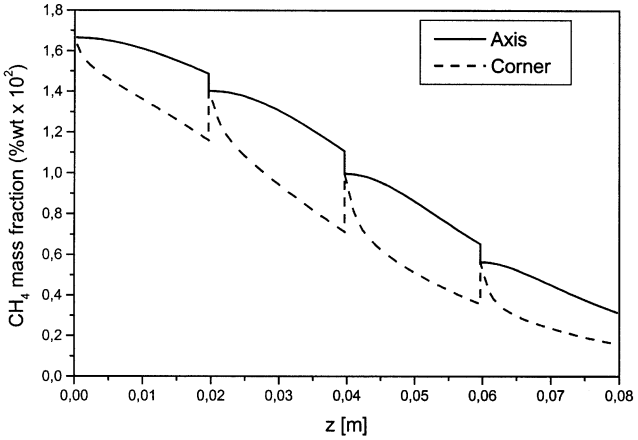

Figure 15. CH_4 mass fraction along the axis and the corner of the channel: segmented-channel model.

though the segmentation causes a leveling of these gradients in the empty spaces between wafers, they develop again quite rapidly in each segment. The larger differences are in the ignition region (second segment). The axial temperature profiles at the same axial and corner positions show similar behavior, with differences as high as 200 degrees already anticipated in Figure 10 for a continuous channel.

Now we intend to ascertain quantitatively how much the process is mass-transfer-controlled in the conditions just simulated. More specifically, we quantified the influence of the diffusion coefficients and kinetic parameters on the progress of overall combustion, measured by the fuel conversion rate. In particular, we monitored the value of the sensitivity index

$$SI(z) = \left(\frac{\partial \chi}{\partial z} - \frac{\partial \chi^0}{\partial z} \right) \Big/ \frac{\partial \chi^0}{\partial z} \qquad (22)$$

as a function of the axial coordinate. Note that the conversion derivative represents the overall fuel combustion rate, so that $SI(z)$ measures its variation following a perturbation of one parameter relative to a reference case (χ^0), with the parameters set to the values used in the previous calculations.

We considered the influence of two parameters separately: the CH_4 diffusion coefficient (D_{CH_4,N_2}) and the preexponential factor (A) in Eq. 10. Each one is used to assess a specific mechanism: the diffusion coefficient of methane allows us to quantify the limitations caused by the slow flux of this reagent to the catalytic walls, while A is a simple means of varying the surface reaction rate (that is, the activity of the catalyst). In the simplified chemistry used to test the model, CH_4 and O_2 are the only reagents, but the much greater abundance of the latter makes even large variations ($+50\%$) of its diffusion coefficient (D_{O_2,N_2}) to result in negligible effects. Moreover, since Eq. 10 assumes irreversible kinetics, the mass-transfer properties of CO_2 and H_2O cannot limit the reaction rate.

We changed the reference parameter values previously used

$$D_{CH_4,N_2} = -2.3840\times10^{-5} + 1.0822\times10^{-7}T + 9.7661\times10^{-11}T^2 \quad m^2/s$$

$$A = 273.85 \quad m^{5/2}/s\cdot kg^{1/2}$$

by $+10\%$, starting from a given axial coordinate onwards. The results of several tests are summarized in Figure 16. Note that increasing either the reaction rate or the methane diffusion coefficient always results in a positive $SI(z)$, which means an acceleration of the combustion rate. It should be observed that the local conversion value—and, thus, also its derivatives and so the sensitivity index $SI(z)$—is affected by the previous history in the channel. Thus, it is meaningless to compare the values of the derivative long after the variation in the parameter occurrred, because all the other variables will have changed significantly, determining completely different conditions with respect to the reference case. The individual influence of the given parameter is indicated by the value of $SI(z)$ soon after the point where the change occurred. Consequently, Figure 16 shows eight different simulations in which D_{CH_4,N_2} or A was changed at the middle of each segment. Note that the sensitivity index is plotted only from the beginning of the reactor up to the end of the segment in which the variation took place, since the remaining profile is of no value, as explained earlier.

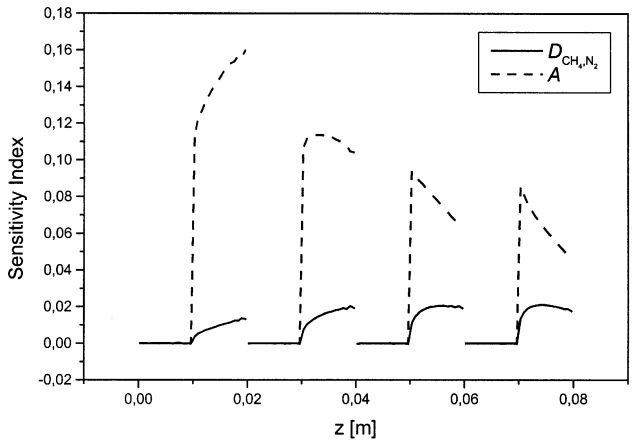

Figure 16. Variations of the sensitivity index, $SI(z)$, after a 10% increase in the preexponential factor A or D_{CH_4,N_2} in the middle of each segment; each curve is a different simulation (8 total).

Figure 16 clearly shows that increasing A by 10% causes almost an order of magnitude larger variation in the combustion rate than does varying D_{CH_4,N_2} by the same relative amount. The influence of the diffusion coefficient is not negligible, anyway. At the same time, we can see that the influence of the chemistry (A) is larger at the beginning, while the role of mass transfer increases later, when the reaction gets faster. This is quite an obvious point, well known in the literature. But Figure 16 proves quantitatively that the role of chemistry always prevails, even with rather active catalysts, as Pt-based are known to be. At the same time, control conditions by either chemistry or mass/heat transfer are never met. Several results similar to those reported in Figure 16 have been obtained at different operating conditions, a concise summary of which is given in the following. A higher base value of the preexponential factor, A, simulating an even more active catalyst, caused the sensitivity to D_{CH_4,N_2} to increase with respect to the sensitivity to A, confirming that mass (and heat) transfer becomes increasingly important processes as the reactions become faster. Still, even doubling A, the sensitivity to A is larger than SI_D, though they are becoming comparable. A larger inlet velocity results in a decrease in the role of D_{CH_4,N_2}, and correspondingly to a higher weight of the surface reaction rate. Applying the variations of the parameter values in different positions inside the segment clearly affects the results, as can be expected by simply inspecting Figure 15. Varying the diffusion coefficient at the entrance of a segment has almost no effect, due to the uniform transverse concentration profile. A warmer feed stream leads to earlier ignition and allows almost complete conversion to be reached in the 0.08-m-long monolith. In this case, the effect of varying the methane diffusion coefficient is greater, and is immediately reflected in the change in com-

bustion rate, though the predominance of the chemistry remains.

We can easily conclude that the case simulated here, based on experimental data in Bond et al. (1996), is never under chemical or mass control, but the importance of the surface reaction is always predominant. We believe that such a conclusion goes beyond the data considered, since the catalyst used in the study of Bond et al. (1996) is one of the most active ones used in methane catalytic combustion.

Fitting the Kinetics to the Experimental Data

According to the results of the sensitivity analysis, the chemical kinetics is a crucial piece of information to model the experimental data of Bond et al. (1996). Note that we reached this conclusion because we used a model that properly accounts for the physical processes, which were found to play a minor role in this case. Still, the complete 3-D model, including segmentation, has to be used to correctly identify an intrinsic surface-reaction model.

As explained earlier, in this work we describe the surface reaction through a global kinetic equation, as frequently reported in the literature. First we checked the partial reaction orders (as reported in Eq. 10) and the kinetic parameters ($A = 4.11 \times 10^7$ $m^{5/2}/s \cdot kg^{1/2}$, $E_a = 134.7$ kJ/mol) claimed in the literature to be typical of catalytic combustion of CH_4/air mixtures (Markatou et al., 1993). These parameters were shown to be (Canu, 2001) not useful for describing the experimental data of Bond et al. (1996). We believe this to be quite an obvious result, due to the limitations of the global reaction approach to the complex, multistep reaction mechanism. In spite of this, the widespread use of a single reaction to model catalytic combustion encouraged us to evaluate the possibility of a single kinetic equation to describe the given experimental data where the chemistry is particularly important.

Based on the standard routines (More et al. 1981) we set up an optimization procedure that uses the segmented 3-D model and the kinetic Eq. 10, allowing for changes in A and E_a. The model is solved over and over, each time varying the values of A and E_a and searching that couple that minimizes the errors in the prediction of the experimental conversion data reported in Table 1. Once again, for repetitive simulations we took advantage of an efficient CFD code with the modifications that we implemented to guarantee a fast and reliable convergence. Again, the commercial program has been modified through its standard features to interface it with Minpack optimization routines.

The best fit was obtained with $A = 112.6$ $m^{5/2}/s$ $kg^{1/2}$, $E_a =$ 54.97 kJ/mol, and the comparison with experimental data is shown in Figure 17 as a dashed line. The simulated curve does not show the pronounced change in concavity that characterized the experimental data. On the other hand, sensitivity analysis clearly pointed out that such a marked decrease in the experimental combustion rate is not entirely due to mass transfer limitations, which weakly influence the process in the second half of the monolith. Besides proving that the global kinetic Eq. 10 is structurally inadequate, the fitting results indicate that some sort of chemical inhibition arises at a higher conversion. The most likely candidate for limiting the surface activity is water, as has been frequently observed

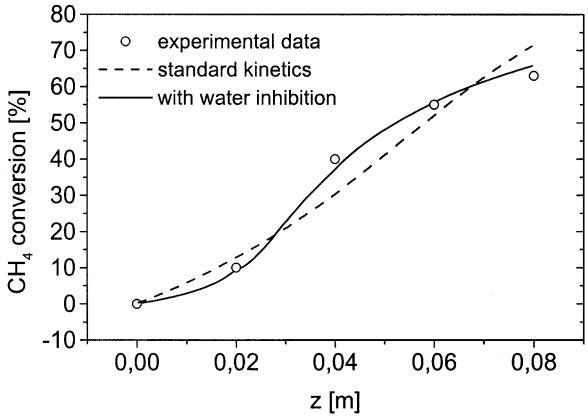

Figure 17. Best fit of experimental CH_4 conversion between subsequent monolith segments.

3-D segmented channel model. Dashed line: varying A and E_a in kinetic Eq. 10; solid line: with inhibition by water, that is, varying A, E_a, A_{ads}, and ΔH_{ads} in kinetic Eq. 23.

(Hayes et al., 1999), since it is thought to compete for the surface site. Water adsorption can be so large to become the most abundant surface species, severely limiting the availability of surface sites for methane and oxygen. Semiempirical modifications of Eq. 10 to include water inhibition through competition for surface sites can be formulated in a Langmuir–Hinshelwood form as

$$R = \frac{A \cdot \exp\left(-\frac{E_a}{RT}\right) \cdot C_{O_2}^{0.5} \cdot C_{CH_4}}{1 + K_{ads} \cdot C_{H_2O}} \tag{23}$$

with

$$K_{ads}(T) = \exp\left(-\frac{\Delta G_{ads}}{RT}\right) \simeq A_{ads} \exp\left(-\frac{\Delta H_{ads}}{RT}\right) \tag{24}$$

In the case of the experimental data of Bond et al. (1996), the water concentration was already relatively high at the inlet, because preheating was obtained through the homogeneous combustion of H_2, added to the CH_4/air mixtures for that purpose. Since CH_4 inlet concentration is quite low (1.67 wt. %), the additional water produced by the reaction even at complete conversion is not very significant. At 63% conversion, the mass fraction of water is 9.3 wt. %, as compared with 6.4 wt. % at the inlet. It seems difficult to accept that such a small variation in water concentration in the monolith could eventually lead to a significant effect. Calculations reveal a surprising result, though, which is shown in Figure 17 together with the previous fitting, based on Eq. 10. Results have been obtained by means of the fitting techniques already mentioned, this time varying the parameters A_{ads} and ΔH_{ads} in kinetic Eq. 23, in addition to A and E_a. The best fit was obtained with the values

$$A = 4.048 \times 10^6 \quad m^{5/2}/s \cdot kg^{1/2} \qquad E_a = 135.4 \quad kJ/mol$$

$$A_{ads} = 3.57 \times 10^{10} \quad m^3/kg \qquad \Delta H_{ads} = -179.3 \quad kJ/mol$$

The effect of the water adsorption term—the denominator in Eq. (23)—is seen on the other parameters as well. Now the activation energy of the surface reaction is found to be higher than that obtained with the simpler Eq. 10, surprisingly approaching the value suggested in the literature (Markatou et al., 1993), where it is used without any water inhibition term, however. At the same time, the value of heat of adsorption of water falls close to the experimental microcalorimetry measurements of McHale et al. (1997) for alumina surfaces, which are reported to range between -30 and -39 kcal/mol ($-125.6 \div -165.3$ kJ/mol). The result in Figure 17 can be seen as quite impressive, but in our opinion it simply confirms the importance of chemical kinetics quantitatively agreeing with the catalytic combustion experimental data in the monolith. Chemistry must be correctly introduced in a detailed model of the flow, heat transport, and geometry. The semiempirical expression of Eq. 23 does not provide a general solution to the chemical kinetics, since we expect its parameters to change, even significantly, with other catalyst and conditions. We agree that the only indication in Figure 17 is that more effort is required to introduce fundamental surface chemistry mechanisms into detailed models of the reacting flow. Our work is advancing in this direction, provided the detailed modeling framework presented in this article is now well assessed and proved to be well worth the effort, due to the relevance of actual details, such as the real reactor geometry. Once the intrinsic surface kinetics are identified, the role of diffusion in the pores of the catalyst (the washcoat, in this case) will be worth evaluating.

Conclusions

The catalytic combustion of a methane/air mixture in a structured catalyst is a relevant application where a localized reaction interacts not obviously with the flow structure. Simultaneous modeling of the fluid flow and reaction is a key problem that CFD can help to solve but at the same time, it is also one of its developing areas. This study focused on ascertaining the appropriate level of detail in chemistry, flow, and geometry modeling, relying on the ease with which the latter can be simulated with commercial CFD codes. The implementation of a localized reaction into a standard CFD code is a significant contribution, particularly with regard to the convergence that can be seriously endangered by a fast, strongly exothermic reaction in a compressible flow, and confined at the domain boundary.

Experimental data in the literature were used to compare simulation results and as a basis for modeling parametric studies. The relevance of temperature-dependent transport properties of a process that spans a wide range of temperatures has been demonstrated and quantified. The diffusion coefficients and N_2 thermal conductivity are the most critical properties, and their evaluation requires some attention.

Different 2-D approximations of the square monolith channel (intrinsically 3-D) have been compared, and the conclusion was that equivalence based on either chemistry (same catalytic surface) or flow (same cross section) does not lead to similar results, and the latter is preferred for the simulated conditions. This proved the relevance of the flow and geometry conditions, particularly with regard to the importance of the chemistry indicated by sensitivity analysis. Turning to 3-D models, it was found that they predict different ignition behavior with respect to 2-D approximations, because of the faster heating at the corners. Thus 3-D models always must be used when the real process has 3-D features, considering that CFD codes allow us to simulate them rather easily. Segmentation of the monolith frequently used for both industrial and laboratory studies has been modeled as well, and its influence on the overall combustion rate was found to be significant, particularly for mass-transfer-limited processes. Advantage has been taken again of the ease with which CFD codes allow us to implement rather complicated boundary conditions and calculate the developing boundary layer following each segment entrance.

The importance of chemical kinetics relative to mass transport has been discussed through sensitivity analysis, in addition to radial profile discussions. It was proved that the decrease in the combustion rate at a higher conversion is mostly a chemical effect, instead of a diffusion limitation, as is usually suggested. It was concluded that there is a need for a better description of the surface mechanism, even if the simulated data are never under complete chemical control.

The robustness of the CFD application that was developed, and the rate of convergence, allowed us to set up a parameter-fitting procedure to carry out kinetic studies based on experimental data. To demonstrate this capability, modification of the classic single-step-rate equation should include inhibition by water, which closely matches the experimental data. Such a result is considered a first step toward the implementation of a more detailed and theoretically based kinetic mechanism and rate equations in the 3-D models.

The overall conclusion is that more detailed surface and gas-phase reaction mechanisms must be included, but only after a comparably detailed model of the momentum and heat transport in the actual geometry of the real process is developed and validated, as was done here. A meaningful kinetic study to properly identify kinetic parameters in elementary step rate equations definitely requires a sufficiently accurate model of the experimental setup and data, where the geometry and flow simulation are crucial. In this view, a commercial CFD code suitably adapted can provide the required flexibility to handle nonidealized geometry and flow structure.

Notation

A = preexponential factor; cross section of the channel, m^2
C = mass concentration, kg/m^3
C_p = specific heat at constant pressure, $J/(kg \cdot K)$
C_v = molar-specific heat at constant volume, $J/(mol \cdot K)$
D = diffusion coefficient, m^2/s
E_a = activation energy, kJ/mol
f = functions of μ_i, $C_{v,i}$, D_{ii}, and T in λ
H = total enthalpy per unit mass, J/kg
h = thermodynamic enthalpy, J/kg
k_B = Boltzmann constant, ergs/K
$\dot{M}$ = total mass flow rate through the channel, kg/s
m_{ik} = reduced molecular mass for the (i,k) species, g
N_r = number of surface reactions
n = right side minus left side of reaction equation
p = pressure, Pa
r = radial coordinate in the 2-D model
R^S = rate of surface reaction, $kg/(m^2 s)$
S = source term in conservation equation
SI = sensitivity index
T = temperature, K; transpose of a vector

u = axial component of velocity, m/s
$\boldsymbol{U}$ = velocity vector of components u, v, and w, m/s
v = transverse component of $\boldsymbol{U}$
w = transverse component of $\boldsymbol{U}$
W = molecular weight, kg/kmol
x,y = transverse coordinates in the 3-D model
Y = mass fraction of species
z = axial coordinate, m
Z = compressibility factor

Greek letters

δ = tensor of versors
λ = thermal conductivity, J/(m·K·s)
μ = molecular viscosity, Pa·s
ν = stoichiometric coefficient
ξ = CH_4 conversion
ρ = mass density, kg/m^3
σ = effective Lennard-Jones collision diameter, Å
ϕ = fuel equivalence ratio: $(kg_{CH_4}/kg_{O_2})/(kg_{CH_4}/kg_{O_2})_{stech}$
χ = conversion of methane, %
Ω = collision integral

Superscripts and subscripts

0 = reference simulation
ad = adiabatic
ads = adsorption
i = species index
in = inlet conditions
j = reaction index
H = enthalpy
mix = of the mixture
p = constant pressure
trans = translational
rot = rotational
v = constant volume
vibr = vibrational

Literature Cited

Boehman, A. L., and R. W. Dibble, "Experimental and Numerical Investigation on the Influence of Temporal Fuel/Air Unmixedness on NOx Emissions of Lean Premixed Catalytically Stabilized and Non-Catalytic Combustion," *Catal. Today*, **59**, 131 (2000).

Bond, T. C., R. A. Noguchi, C. P. Chou, R. K. Mongia, J. Y. Chen, and R. W. Dibble, "Catalytic Oxidation of Natural Gas Over Supported Platinum: Flow Reactor Experiments and Detailed Numerical Modelling," *Proc. of the Int. Symp. on Combustion*, Naples, Italy, The Combustion Institute, University Park, PA, p. 1771 (1996).

Boudart, M., and G. Djega-Mariadassou, *Kinetics of Heterogeneous Catalytic Reactions*, Princeton Univ. Press, Princeton, NJ (1984).

Canu, P., "Simulation and Interpretation of Catalytic Combustion Experimental Data," *Catal. Today*, **64**, 239 (2001).

Deutschmann, O., F. Behrendt, and J. Warnatz, "Modelling and Simulation of Heterogeneous Oxidation of Methane on a Platinum Foil," *Catal. Today*, **21**, 461 (1994).

Dixon-Lewis, G., "Flames Structures and Flame Reaction Kinetics. Transport Phenomena in Multicomponent Systems," *Proc. Roy. Soc. A*, **304**, 111 (1968).

Dryer, F. L., and I. Glassman, "High-Temperature Oxidation of CO and CH_4," *Proc. of the Int. Symp. on Combustion*, The Combustion Institute, University Park, PA p. 987 (1972).

Dumesic, J. A., D. F. Rudd, L. M. Aparicio, J. E. Rokoske, and A. A. Treviño, *The Microkinetics of Heterogeneous Catalysis*, American Chemical Society, Washington, DC (1993).

Forzatti P., and G. Groppi, "Catalytic Combustion for the Production of Energy," *Catal. Today*, **54**, 165 (1999).

Furuya, T., T. Hayata, S. Yamanaka, J. Koezuka, T. Yoshine, and A. Ohkoshi, "Hybrid Catalytic Combustors for Gas Turbine Applications," ASME Gas Turbine Conf. and Exhibition, Anaheim, CA, (1987).

Frenklach, M., H. Wang, M. Goldberg, G. P. Smith, D. M. Golden, C. T. Bowman, R. K. Hanson, W. C. Gardiner, and V. Lissianski, GRI Report No. GRI-95/0058, Gas Research Institute (GRI), Des Plaines, IL (1995).

Geus, J. W., and J. C. van Giezen, "Monolith in Catalytic Oxidation," *Catal. Today*, **47**, 169 (1999).

Groppi, G., A. Belloli, E. Tronconi, and P. Forzatti, "A Comparison of Lumped and Distributed Models of Monolith Catalytic Combustors," *Chem. Eng. Sci.*, **50**, 2705 (1995).

Hayes, R. E., S. T. Kolaczkowski, and W. J. Thomas, "Finite-Element Model for a Catalytic Monolith Reactors," *Comput. Chem. Eng.*, **16**, 645 (1992).

Hayes, R. E., and S. T. Kolaczkowski, "Mass and Heat Transfer Effects in Catalytic Monolith Reactors," *Chem. Eng. Sci.*, **49**, 3587 (1994).

Hayes, R. E., and S. T. Kolaczkowski, "A Study of Nusselt and Sherwood Numbers in a Monolith Reactors," *Catal. Today*, **47**, 295 (1999).

Hayes, R. E., S. Awdry, and S. T. Kolaczkowski, "Catalytic Combustion of Methane in a Monolith Washcoat: Effect of Water Inhibition on the Effectiveness Factors," *Can. J. Chem. Eng.*, **77**, 688 (1999).

Hirschfelder, J. O., C. F. Curtiss, and R. B. Bird, *Molecular Theory of Gases and Liquids*, Wiley, New York (1954).

Jahn, R., D. Snita, M. Kubicek, and M. Marek, "3D Modelling of Monolith Reactors," *Catal. Today*, **38**, 39 (1997).

Kee, R. J., G. Dixon-Lewis, J. Warnatz, M. E. Coltrin, and J. A. Miller, "A Fortran Computer Code Package for the Evaluation of Gas-Fase Multicomponent Transport Properties," *Report SAND86-8246*, Sandia National Laboratories, NM (1994).

Kolaczkowski, S. T., "Modelling Catalytic Combustion in Monolith Reactors—Challenges Faced," *Catal. Today*, **47**, 209 (1999).

Markatou, P., L. D. Pfefferle, and M. D. Smooke, "A Computational Study of Methane-Air Combustion Over Heated Catalytic and Non-Catalytic Surfaces," *Combust. Flame*, **93**, 185 (1993).

McHale, J. M., A. Auroux, A. J. Perrotta, and A. Navrotsky, "Surface Energies and Thermodynamic Phase Stability in Nanocrystalline Aluminas," *Science*, **277**, 788 (1997).

More, J. J., B. S. Garbow, and K. E. Hillstrom, "Fortran Subroutines for Testing Unconstrained Optimization Software," *ACM Trans. Math. Software*, **7**, 136 (1981).

Ozawa, Y., J. Hirano, M. Sato, M. Saiga, S. Watanabe, and M. Okahata, "Preliminary Tests Results of Catalytic Combustor for Gas Turbine," *Proc. JECAT '91*, Tokyo, p. 30 (1991).

Patankar, S. V., *Numerical Heat Transfer and Fluid Flow*, McGraw-Hill, New York (1980).

Pfefferle, L. D., "Heterogeneous/Homogeneous Reactions and Transport Coupling for Catalytic Combustion Systems: A Review of Model Alternatives," *Catal. Today*, **26**, 255 (1995).

Raja, L. L., R. J. Kee, O. Deutschmann, J. Warnatz, and L. D. Schmidt, "A Critical Evaluation of Navier-Stokes, Boundary-Layer, and Plug-Flow Models of the Flow and Chemistry in a Catalytic-Combustion Monolith," *Catal. Today*, **59**, 47 (2000).

Young, L. C., and B. A. Finlayson, "Mathematical Models of the Monolith Catalytic Converter: 1. Development of Model and Application of Orthogonal Collocations," *AIChE J.*, **22**, 331 (1976).

Wilson, R., A. Bardon, and J. Witton, "Experimental and Computational Investigation of Flow in Catalytic Monolith Channels," *Proc. Int. Gas Turbine and Aeroengine Congress and Exposition*, Cologne, Germany (1992).

Manuscript received Dec. 17, 2001, and revision received May 20, 2002.